

Network simulation for deep bed filtration of Brownian particles

You-Im Chang^{a,*}, Shan-Chih Chen^b, Hsun-Chih Chan^a, Eric Lee^b

^aDepartment of Chemical Engineering, Tunghai University, P.O. Box 833, Taichung 40704, Taiwan, ROC

^bDepartment of Chemical Engineering, National Taiwan University, Taipei 10617, Taiwan, ROC

Received 26 September 2003; received in revised form 10 June 2004; accepted 14 July 2004

Available online 17 August 2004

Abstract

The effect of different interaction energy curves of DLVO theory on the permeability reduction in a filter bed is investigated by using the Brownian dynamics simulation method and the modified square network model to track the individual particles movement through the filter bed. When energy barrier exists and both particle and pore size distributions are of the Raleigh type, it is found that particles with Brownian motion behavior are easier to get straining at small pores, and cause higher permeability reduction than those without considering the Brownian motion behavior. But, this result was not observed for the constant particle and pore sizes case. The permeability reduction for the Raleigh size distribution is higher than that of the constant size. Similar results are also obtained for the “barrierless” type interaction energy curve for the case of Raleigh type size distribution, with the exception that the decreasing rate of permeability reduction of Brownian particles is smaller than that without considering the Brownian motion behavior. When comparing with the permeability reduction experimental data, it is found that the present model shows fair agreement between the theory and the experimental results when the direct deposition mechanism is dominant.

© 2004 Elsevier Ltd. All rights reserved.

Keywords: Filtration; Network; Simulation; Particle; Brownian motion; Porous media

1. Introduction

The transport of particulate suspension through porous media and the deposition of particles onto the pore walls are considerable industrial and theoretical interests. For example, in the production of potable water by deep bed filtration process, colloidal particles deposit on the surfaces of grains caused by the complex interactions between the particle surfaces and the granular collectors (Tien, 1989), and consequently, the permeability of the filter is reduced. The permeability reduction rate along the filter bed is dependent on several system parameters which are the subjects of numerous studies, and those parameters are: the fluid superficial velocity and the grain and particle sizes (Ison and Ives, 1969; Herzog et al., 1970; Yao et al., 1977), the geometry of collector (Tien and Payatakes, 1979), the interaction forces between particles and collector surfaces

(Kim and Rajagopalan, 1982; Chang and Whang, 1998), and the pore size distribution (Sharma and Yortsos, 1987; Rege and Fogler, 1988; Imdakm and Sahimi, 1991; Chang et al., 2003).

Generally, there are two theoretical approaches of predicting the deposition rates of colloidal particles on to the granular surfaces (i.e. collector), namely Eulerian and Lagrangian (Russel et al., 1989). For the Eulerian method, the deposition rates of colloidal particles on the collector surfaces are considered to be governed by the convective diffusion equation which was well established by Prieve and Ruckenstein (1974), and Spielman and Friedlander (1974). The paper published by Elimelech (1994) provides the detailed numerical technique to solve this convective diffusion equation. Contrary to the Eulerian approach, the Lagrangian approach can determine the trajectory of a particle by calculating the force balance and the torque balance on the particle (Tien, 1989). Hence, by knowing the hydrodynamic flow field around the collector surfaces, for example, the constricted tube model established by Payatakes et al. (1973),

* Corresponding author. Tel.: +886-93349006; fax: +886-423590009.
E-mail address: yichang@mail.thu.edu.tw (Y.-I. Chang).

one can describe the particle's path near a collector surface. And then by applying the concept of the limiting trajectory (Spielman and FitzPatrick, 1973), the deposition rates of particles can be determined. However, since this trajectory equation is deterministic and the Brownian diffusion force was not considered, hence the Brownian motion of particles (which is stochastic in nature) cannot be described in their deposition behavior. Inclusion of these random forces in this Lagrangian type trajectory equation leads to a Langevin type equation, which was solved successfully by Kanaoka et al. (1983) and Gupta and Peters (1985). As described in the dissertation of Rajagopalan (1974), when the inertia term in the force balanced equation is ignored, there is a direct relationship between the Langevin equation and the convective diffusion equation via the Fokker–Planck–Kolmogorov equation, and the equivalent Ito form of the Stratonovich differential equation. With the aid of this Langevin type equation and the concept of the control window (Wang et al., 1977; Pendse et al., 1978), a stochastic simulation method describing the deposition behavior of Brownian particles was successfully established by Ramarao et al. (1994), and this method will be adopted in the present paper.

In order to describe the effect of pore size distribution on the particle deposition behavior along the filter bed properly, the network model has been applied extensively to simulate the formation of porous media since the pioneer work of Todd et al. (1984) 20 years ago. A review paper describing the continuum and discrete models of particle transport and gas reaction processes in disordered porous media was given by Sahimi et al. (1990), at which the statistical physics of disordered media was well described, and the topology of porous media can be defined by using the coordination number Z ; for example, $Z = 4$ stands for a simple square network model and $Z \rightarrow \infty$ stands for a parallel capillary tube network in a two-dimensional coordinate. Applying this coordination number and the conductance calculation method of the effective medium approximation (EMA) (Kirkpatrick, 1973), Sharma and Yortsos (1987) had successfully established a set of population balance equations, and calculated the temporal variations of the filter coefficient caused by the particle deposition in a filter bed. In their model, two types of particle deposition mechanisms, straining and direct deposition, were being considered in the capillary tube model. The permeability reductions resulting from particle's deposition were then calculated by using EMA, where the fluid velocity is assumed to be the same in all pore throats of a given size in the network. Then, applying the principle of flow biased probability and the concept of wave front movement, both Rege and Fogler (1988) and Imdakm and Sahimi (1991) predicted the permeability and the effluent concentration of particles, and were in good agreement with the available experimental data. Later on, by viewing the void space of porous media as a constricted tube unit bed element (UBE), Burganos et al. (1992) had developed a three-dimensional network simulator to calculate the filter coefficient, at which the deposition rate of particles is determined

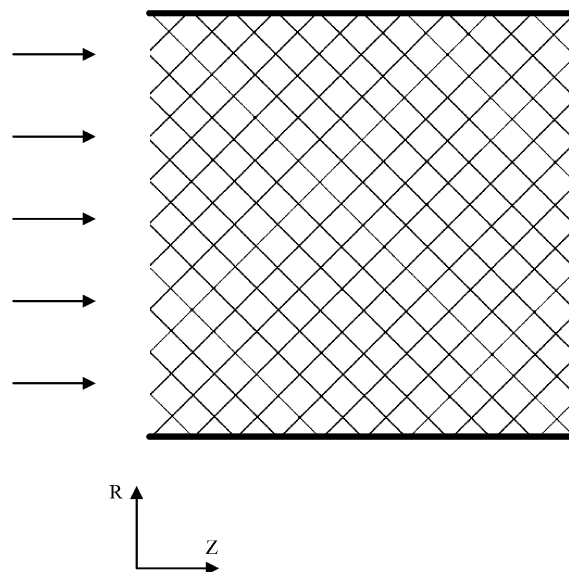


Fig. 1. The simple modified square network model.

by using the method of trajectory analysis. But, in their force balanced equations, the Brownian diffusion force of particles was not considered.

In the present paper, with the adoption of the Brownian dynamic simulation method mentioned above, we used the two-dimensional modified square network model (see Fig. 1) to track the individual particles with Brownian motion behavior as they move through the filter bed. From which, caused either by the straining or by the direct deposition of particles on the pore walls, the temporal variations of the permeability reduction and the pressure drop can be determined. The type of sinusoidal constricted tube (SCT) will be adopted in the present simulation. In addition, the effects of the total interaction energy curve of DLVO theory with various shapes (Verwey and Overbeek, 1948) are also investigated. The permeability reduction predicated by our model shows good agreement with the available experimental data of Soo and Radke (1984) and Soo et al. (1986) and Stephan and Chase (2003).

2. Network model

In the present study, we use the modified two-dimensional square network (as shown in Fig. 1) to represent the porous media of the filter, and adopt the Brownian dynamic simulation method to track the individual particles as they move through the network. In Fig. 1, all bonds (i.e. pores) in the network are assumed to have the same length, but with a Raleigh form pore size distribution (Sharma and Yortsos, 1987):

$$f_p(r') = 2r' \exp(-r'^2), \quad (1)$$

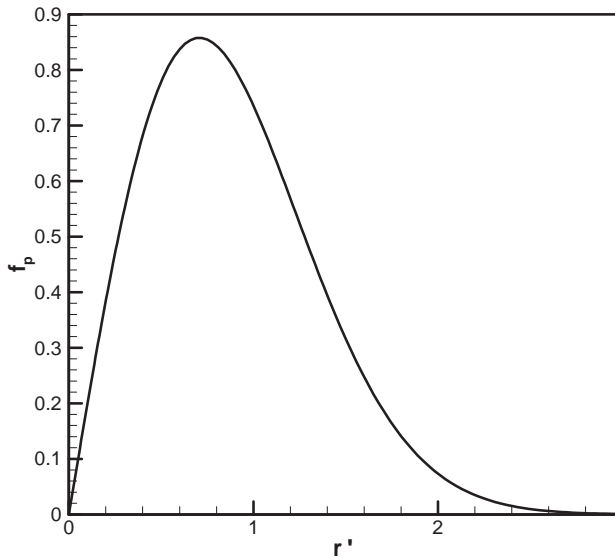


Fig. 2. The size distribution of the Raleigh form.

where f_p and r' are the dimensionless distribution density and the dimensionless radius of pores, respectively. Eq. (1) satisfies the following equation:

$$\int_0^{\infty} 2r' \exp(-r'^2) dr' = 1. \quad (2)$$

This distribution can then be assigned randomly to the bonds in the network as follows:

$$\int_0^{r'_1} 2r' \exp(-r'^2) dr' = 1 - \exp(-r'_1{}^2) \quad (3)$$

with

$$r'_1 = \frac{r_f}{r_{\text{mean}}} = \sqrt{-\ln(1 - a_i)} \quad (4)$$

and

$$0 < a_i < 1,$$

where the random number a_i can be generated by using the standard computer software (IMSL, 1985) and r_{mean} is the mean radius of pores. A typical diagram of Raleigh distribution is shown in Fig. 2. Eq. (4) can also be applied to determine the particle size distribution randomly in the computer simulations described as follows.

As particles of a given size distribution transport through a bond shown in Fig. 1, they will arrive at a node where the fluid will be separated by two paths to flow further into the network. In the present study, we adopt the method of flow biased probability to determine either one path for particles to flow through (Rege and Fogler, 1988). As shown in Fig. 1, when a particle encounters a node in the network, it has a choice of exit path. The exit path is selected randomly in the present model, but with a bias toward the paths with greater flow rates. Usually, the greater the flow rate, the greater the probability of the particle choosing that path.

Details of this method can be found elsewhere (Rege, Ph.D. Thesis, 1988).

In the current model, two different mechanisms of particle capture are considered: straining (size exclusion) and direct deposition. Straining occurs when the particle diameter is larger than the pore diameter selected for it to transport through the network. Straining plugs up the pore and drops its permeability to zero, and thereby changing the flow direction to other available pores. Direct deposition of a particle on a pore wall occurs as a result of hydrodynamic and DLVO interaction forces acting on the particle. Details of this direct deposition mechanism in a constricted tube cell are given as follows.

3. Constricted tube cell

We represent the pore geometry of bonds in the present network by the constricted tube type cell (Payatakes et al., 1973). The dimension of this cell is characterized by three quantities: the height, h , the maximum diameter, d_{max} , and the constriction diameter, d_c . The radius r_c and r_{max} are $d_c/2$ and $d_{\text{max}}/2$, respectively. Expressions for the determination of these quantities are summarized in Table 1. A schematic representation is shown in Fig. 3. For a spherical collector with diameter d_f , the relationship between r_c , r_{max} and d_f are defined as (Tien, 1989):

$$r_c = \frac{d_c}{2} = \frac{1}{2} \frac{\langle d_c \rangle}{\langle d_f \rangle} d_f, \quad (5)$$

$$r_{\text{max}} = \frac{d_{\text{max}}}{2} = \frac{1}{2} \left[\frac{\varepsilon(1 - S_{wi}) \langle d_f^3 \rangle}{(1 - \varepsilon) \langle d_c^3 \rangle} \right]^{1/3} d_f, \quad (6)$$

Table 1

Summary of expressions for porous media characterization based on the constricted tube model

Quantity	Expression
Length of periodicity, l_f	$\left[\frac{\pi}{6(1-\varepsilon)} \right]^{1/3} \langle d_f \rangle$
Number of unit cells per unit bed element, N_c	$\frac{6\varepsilon(1-S_{wi})}{\pi \langle d_c^3 \rangle} \left[\frac{\langle d_c \rangle - \varepsilon \langle d_c^3 \rangle}{\varepsilon(1-S_{wi}) \langle d_c^3 \rangle} \right]^{2/3}$
Height, h	d_f
Minimum diameter, d_c	$\frac{\langle d_c \rangle}{\langle d_f \rangle} d_f$
Maximum diameter, d_{max}	$\left[\frac{\varepsilon(1-S_{wi}) \langle d_f^3 \rangle}{(1-\varepsilon) \langle d_c^3 \rangle} \right]^{1/3} d_c$
Volumetric flowrate in a given type of unit cell, q_i	$\frac{u_s}{N_c}$

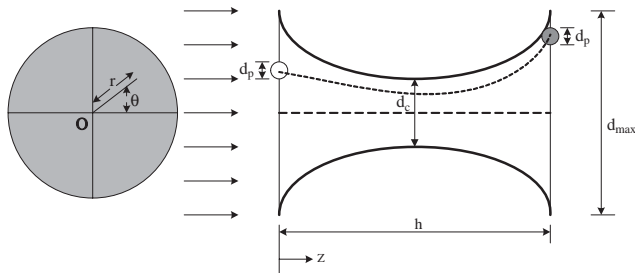


Fig. 3. The schematic diagram of the control window for simulating deposition of Brownian particles in a constricted tube model.

where ε denotes the porosity of porous media, $\langle d_f \rangle$ and $\langle d_c \rangle$ are the mean values of the diameter of spherical collectors and pore constrictions, respectively, and $\langle d_f^3 \rangle$ and $\langle d_c^3 \rangle$ are the mean values of d_f^3 and d_c^3 , respectively. In Eq. (6), S_{wi} represents the fraction of the irreducible saturation of porous media, and its value is 0.111 for glass bead collectors and 0.127 for sand grain collectors (Payatakes et al., 1973). In the present study, the filtration bed is assumed to be packed with sand grains.

The sinusoidal geometric structure (SCT) used by Fedkiw and Newman (1977) is considered for the constricted tube model in the present study. The expressions of the wall radius r_w corresponding to this geometric structures is

$$r_w = \frac{r_c + r_{\max}}{2} \left[1 + \left(\frac{r_{\max} - r_c}{r_{\max} + r_c} \right) \cos \left(2\pi \frac{z}{l_f} \right) \right] \quad (7)$$

for $0 < \frac{z}{l_f} < 1$.

In the present study, the flow field equations established by Chow and Soda (1972) and modified by Chiang and Tien (1985) are adopted. The details of these flow field equations can be found in the book of Prof. Tien (1989).

4. Brownian dynamics simulation

Similar to the previous papers of Ramarao et al. (1994) and authors (Chang and Whang, 1998; Chang et al., 2003), applying the principle of trajectory analysis, the method of Brownian dynamics simulation is adopted in the present study. Assume that the distribution of the initial position (r_{in} , θ_{in}) of each particle is assigned by the random number generator in the flow field simulation. Note that the inlet positions of particles are located at $0 < r_{in} < r_0$ and $0 < \theta_{in} < 2\pi$ (see Fig. 3), at which r_0 is the radial distance beyond which no particle can be placed at the tube inlet (or control window), and r_0 can be found to be

$$r_0 = \frac{d_{\max} - d_p}{2}. \quad (8)$$

With consideration of the inertia term in the force balance equation and of the specification of the flow fluid around

the collector, the particle trajectory can be determined by integrating the Langevin equation as shown below.

The particle velocity vector is represented as (Chang and Whang, 1998; Chang et al., 2003)

$$V = \left\{ [V_0 e^{-\beta t} + U(1 - e^{-\beta t})] F_2(H) + R_v(t) + \frac{1}{\beta} \left(\frac{F_{LO} + F_{DL}}{m_p} \right) (1 - e^{-\beta t}) \right\} F_1(H) F_3(H) \quad (9)$$

with

$$R_v(t) = \int_0^t e^{\beta(\zeta-t)} A(\zeta) d\zeta,$$

where V_0 is the initial velocity of particles, m_p is the mass of the particle, U is the fluid velocity vector, β is the friction coefficient per unit mass of particle, and $F_1(H)$, $F_2(H)$, and $F_3(H)$ are the retardation factors of normal vector, drag force, and shear vector, respectively (Spielman and FitzPatrick, 1973; Elimelech, 1994). Substituting dZ/dt for V with the initial condition $S = S_0$ at $t = 0$, the trajectory equation of particles can be expressed as

$$Z = Z_0 + \left\{ \frac{V_0}{\beta} (1 - e^{-\beta t}) + U \left[t - \frac{1}{\beta} (1 - e^{-\beta t}) \right] \right\} \times F_1(H) F_2(H) F_3(H) + \left\{ R_r(t) + \left(\frac{F_{LO} + F_{DL}}{\beta m_p} \right) \times \left(t + \frac{e^{-\beta t}}{\beta} - \frac{1}{\beta} \right) \right\} F_1(H) F_3(H) \quad (10)$$

with

$$R_r(t) = \int_0^t \left[\int_0^n e^{\beta\zeta} A(\zeta) d\zeta \right] e^{-\beta n} dn,$$

where $A(t)$ represents a Gaussian white noise process in stochastic terms. $R_v(t)$ and $R_r(t)$ are two random deviates which are bivariate Gaussian distribution. The details of $R_v(t)$ and $R_r(t)$ can be found in Kanaoka et al. (1983) and Ramarao et al. (1994). In order to avoid the artificial tunneling error occurring in the numerical integration of dZ/dt , the value of the time step Δt adopted in the present paper remains as small as 10^{-6} s, which is the same order of the momentum time ($\sim 1/\beta$) of the particle (Gupta and Peters, 1985).

In Eqs. (9) and (10), F_{LO} and F_{DL} are the van der Waals force and the electrostatic repulsion force interacting between the particle and the collector surface, respectively as

$$F_{LO} = -\nabla \phi_{LO}, \quad F_{DL} = -\nabla \phi_{DL} \quad (11)$$

with

$$\phi_{LO} = -N_{LO} \left[\frac{2(H+1)}{H(H+2)} + \ln H - \ln(H+2) \right]$$

(with the unit of $k_B T$),

$$\phi_{DL} = N_{E1} \left\{ N_{E2} \ln \left[\frac{1 + \exp(-X)}{1 - \exp(-X)} \right] + \ln[1 - \exp(-2X)] \right\}$$

(with the unit of $k_B T$) hence:

$$F_{LO} = -\frac{2A}{3r_p} \left[\frac{1}{(H^2 + 2H)^2} \right] \quad (12)$$

$$F_{DL} = \frac{2k_B T}{r_p} N_{E1} (N_{DL} e^{-N_{DL} H}) \left\{ \frac{N_{E2} - e^{-N_{DL} H}}{1 - e^{-2N_{DL} H}} \right\}, \quad (13)$$

where $H = h_s/r_p$, $N_{LO} = A/6k_B T$, $N_{DL} = \kappa r_p$, $X = N_{DL} H$,

$$N_{E1} = \frac{v r_p (\varphi_1^2 + \varphi_2^2)}{4k_B T},$$

$$N_{E2} = \frac{2(\varphi_1 \varphi_2)}{[1 + (\varphi_1/\varphi_2)^2]}. \quad (14)$$

In the above equation, h_s is the smallest separation distance between the particle and the collector surface, A is the Hamaker constant, k_B is the Boltzmann constant, T is the absolute temperature, κ is the reciprocal of the electric double layer thickness, v is the dielectric constant of the fluid, and φ_1 and φ_2 are the surface (zeta) potentials of the particle and the collector, respectively. The algebraic sum of the van der Waals and double-layer potentials gives the total interaction energy curve of the DLVO theory (i.e. $V_T/k_B T = \phi_{LO} + \phi_{DL}$) (Verwey and Overbeek, 1948). In this total interaction energy profile, the existence of two characteristic energy barriers (i.e. the height of the primary maximum and the depth of the secondary minimum) is important in determining the permeability reduction K/K_0 as discussed below.

At each time step, if the distance between the approaching particle and the pore wall is smaller than the diameter of the particle, then this particle is assigned as the “captured” particle. When a particle is captured in a bond of the network, the increase of the pressure drop in that bond can be calculated by the following equation (Happel and Brenner, 1983):

$$\Delta P_p = \frac{12\mu r_p U_0}{r_{f0}^2} \left[1 - \left(1 - \frac{r_p}{r_{f0}} \right)^2 \right]^2 K_1 \quad (15)$$

and

$$K_1 = \frac{1 - \frac{2}{3}(r_p/r_{f0})^2 - 0.20217(r_p/r_{f0})^5}{1 - 2.1050(r_p/r_{f0}) + 2.0865(r_p/r_{f0})^3 - 1.7068(r_p/r_{f0})^5 + 0.72603(r_p/r_{f0})^6}, \quad (16)$$

where U_0 and r_{f0} are the fluid velocity at the centerline and the initial radius of the bond, respectively. Then, the total pressure drop through the bond is given by

$$\Delta P_{\text{total}} = \Delta P_{\text{tube}} + \Delta P_p, \quad (17)$$

where ΔP_{tube} can be calculated by using the Hagen–Poiseuille equation:

$$\Delta P_{\text{tube}} = \frac{16\mu l_f U_0}{r_{f\text{new}}^2}. \quad (18)$$

In Eq. (18), when there are N particles captured in the bond, the new radius of the bond $r_{f\text{new}}$ can be related to the r_{f0} by Rege and Fogler (1988) and Choo and Tien (1995):

$$\frac{1}{r_{f\text{new}}^4} = \frac{1}{r_{f0}^4} + \frac{0.75}{r_{f0}^4} \sum_{i=0}^N \frac{r_{pi}}{l_f} \left[1 - \left(1 - \frac{r_{pi}}{r_{f0}} \right)^2 \right]^2 K_1, \quad (19)$$

where l_f is the length of periodicity of the constricted tube cell (the definition is given in Table 1).

When $r_{f\text{new}}$ of a bond is smaller than $3.0a_p$, this bond is then assumed to be blocked by the captured particles in the present study (Choo and Tien, 1995).

The equation used to estimate the change in the local permeability in the i th bond as the function of deposited particles is (Tien, 1989)

$$K_i = \frac{\varepsilon_i^3 \langle d_f \rangle^2}{180(1 - \varepsilon_i)^2}, \quad (20)$$

where ε_i is the local porosity of the i th bond, which can be calculated by

$$\varepsilon_i = \frac{V_{fi}}{V_{f0}} \varepsilon_0 = \frac{r_{f\text{new}}^2}{r_{f0}^2} \varepsilon_0 \quad (21)$$

with $V_{fi} = \pi r_{fi}^2 l_{fi}$, where ε_0 is the initial porosity of the i th bond. If there are N_L bonds in the network, then the overall permeability of the filter bed with length L is

$$K = \frac{\sum_{i=1}^{N_L} K_i}{N_L}. \quad (22)$$

In order to express the extent of permeability reduction as filtration proceeds, we use the permeability ratio K/K_0 as the function of the pore volumes of fluid injected into the filter bed. Here, the pore volume (p.v.) of the injection fluid is defined as

$$\text{p.v.} = \frac{U_{\text{in}} t}{\varepsilon_0 L} = \frac{C_{\text{in}} V_f}{V_p} \quad (23)$$

with $V_f = \sum_{i=1}^{N_L} \pi r_{fi}^2 l_{fi}$ and $V_p = \sum_{i=1}^{N_L} \frac{4}{3} \pi r_{pi}^3$, where U_{in} is the influent flow rate, C_{in} is the influent concentration

of particles and r_{pi} is the mean radius of influent particles. The size distribution of the i th particle is governed by the random number a_i as (see Eq. (4)):

$$r_{pi} = r_{pm} \sqrt{-\ln(1 - a_i)}. \quad (24)$$

Table 2
Parameter values adopted in the theoretical simulation of the present paper

Parameters	Value
K_B	1.38×10^{-16} erg/K
ε	0.40
μ	1 cp
T	293 K
ρ_f	1 g/cm^3
ρ_p	1 g/cm^3
D_f	$20 \text{ }\mu\text{m}$
D_p	$1 \text{ }\mu\text{m}$
S_{wi}	0.127
C_{in}	1000 ppm
U_m	0.1 cm/s

The local Reynolds number at the i th bond is defined as

$$(N_{Re})_i = \frac{\rho_f h_i u_i}{\mu} \quad \text{with } h_i = d_f,$$

$$\frac{u_i t}{\varepsilon_i l_{fi}} = \frac{(C_{in})_i V_{fi}}{V_{pi}}. \quad (25)$$

Therefore, the averaged Reynolds number of the whole filter can be written as

$$(N_{Re})_{avg} = \frac{\sum_{i=1}^{N_L} (N_{Re})_i}{N_L}. \quad (26)$$

In the present paper, because the superficial velocity of fluid is kept at 0.1 cm/s (see Table 2), hence the initial value of $(N_{Re})_{avg}$ is as small as 0.02, and this value will not become larger than 0.03 when $r_{f_{new}}$ of a bond is smaller than $3.0a_p$ (i.e. this bond is then assumed to be blocked by the captured particles as described above). Therefore, the flow field will be always in the laminar flow region, and the hydrodynamic equations of the constricted tube model established by Chow and Soda (1972) can be used in the present simulation.

5. Simulation results and discussion

An overall description of the simulation procedure is presented in the algorithm shown in Fig. 4, and the values of corresponding parameters are given in Table 2. Simulations are performed on a two-dimensional network with $N_L = 70 \times 70$, and the influent flow rate is kept at constant. The estimation of the permeability ratio K/K_0 based on the Brownian trajectory analysis and the stochastic simulation procedure for different types of DLVO interaction energy curves will be given below at first. Then, by comparing with the available experimental data obtained by Soo and Radke (1984), Soo et al. (1986), and Stephan and Chase (2003), the accuracy of the present simulation method will be discussed in a later section.

5.1. Effect of the interaction energy curve

The effects of the four types of interaction energy curves on the permeability ratio will be investigated in the present section. As shown in Fig. 5, curve *A* exhibits a large primary maximum and a deep secondary minimum; curve *B* displays a large primary maximum and a negligible secondary minimum; while curve *C* has a deep secondary minimum only and a “barrierless” interaction energy curve is represented by curve *D*. In this figure, $N_{E1} = 105.0$ and $N_{DL} = 10.75$ for curve *A*, $N_{E1} = 50.0$ and $N_{DL} = 5.02$ for curve *B*, $N_{E1} = 77.0$ and $N_{DL} = 10.0$ for curve *C*, $N_{E1} = 0.0$ and $N_{DL} = 0.0$ for curve *D*, and $N_{E2} = 1.0$ and $N_{L0} = 7.0$ for all four curves. Our previous paper (2003) calculated the collection efficiencies of particles in SCT, and found that the collection efficiency of curve *D* is always greater than that of other three curves when Reynolds number of fluid is small because there no energy barrier exists, and the deposition mechanism of particles is controlled by the Brownian diffusion effect. For curves *A*, *B* and *C*, it was found that, even with the presence of the deep secondary minimum which increases the accumulation probability of particles for curves *B* and *C*, the steepest slope between the secondary minimum and the primary maximum energy barriers of curve *A* is still the main reason for its lowest collection efficiency among these three curves. But, when Reynolds number becomes large, because of a greater sweep away probability caused by the tangential fluid convection force acting on those particles accumulating at the secondary minimum, the collection efficiency of curve *C* is smaller than that of curve *B*.

Corresponding to curve *A* in Fig. 5, the simulation results of the permeability ratio as the function of pore volumes injected are given in Fig. 6a. In this figure, the case that the particle and pore sizes are of the Raleigh distribution and the constant value case are considered with the Brownian diffusion effect included. For the case of the Raleigh type distribution, both the large primary maximum of curve *A* and the Brownian diffusion effect are unfavorable for the particles to deposit on the pore walls, and particles with Brownian motion behavior can transport more particles into the network and increase the probability of straining small pores, consequently can cause a higher permeability reduction than that without considering Brownian diffusion effect. But, this result is not observed for the case when both the particle size and the pore size are fixed at a constant value. Also, because of the straining effect, the permeability ratio for the case of Raleigh distribution is always lower than the case of a constant size value. Between the distribution of pore size and of particle size, our simulation showed that the pore size distribution has bigger effect on reducing the permeability ratio than that of the particle size distribution. In the above simulations, we found that straining is the main mechanism to reduce the permeability at the initial period of injection for the case of Raleigh distribution, and vice versa for the case of constant size value where the direct deposition mechanism becomes dominant. This result can explain why the

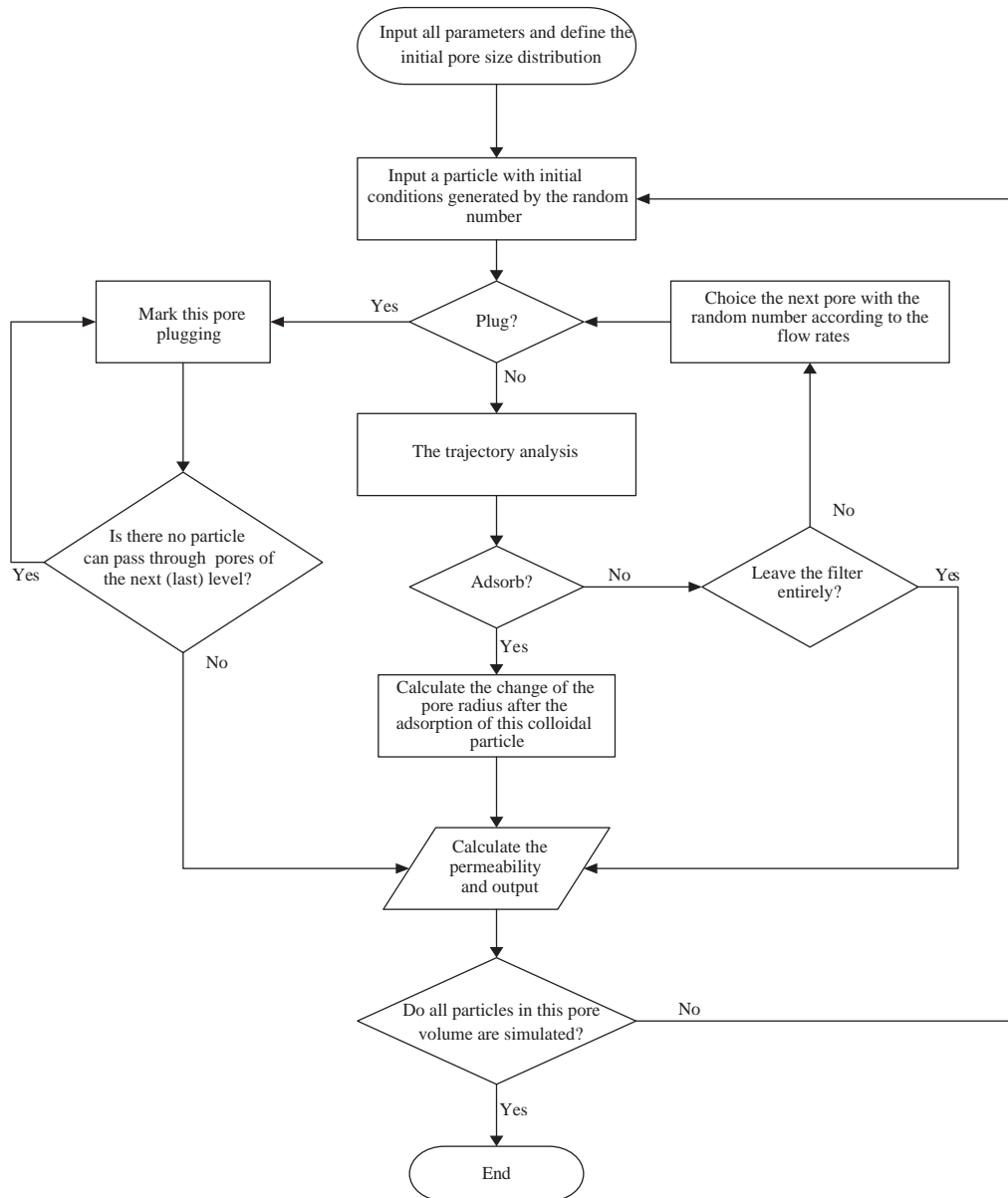


Fig. 4. Flow sheet of the number algorithm for the present computer simulation.

initial decreasing rate of K/K_0 for the case of Raleigh distribution is higher than that of the case of constant size value as shown in Fig. 6a. Corresponding to Fig. 6a, the simulation results of pressure drop are shown in Fig. 6b. Those particles with Brownian motion behavior and with a Raleigh size distribution own the highest pressure drop among these four cases investigated.

Corresponding to the “barrierless” curve D (which favors particle’s deposition), the relationships between the permeability ratio and the pore volumes injected are shown in Fig. 7a. Similar to results shown in Fig. 6a, the permeability ratio for the case of Raleigh distribution is lower than that of the case of a constant size value. The pore size distribution and the straining mechanism still dominate the reduction of

the permeability at the initial period of filtration. But, for the case of Raleigh type distribution when the Brownian diffusion effect is considered, because those Brownian particles can spread wider over the bonds at the entrance region in the network, hence its decreasing rate of permeability ratio is smaller than the case without considering the Brownian diffusion effect as shown in Fig. 7a. Similar result is obtained for the case of constant size value. Corresponding to Fig. 7a, the pressure drop simulation results are shown in Fig. 7b. Among which, the case of Raleigh distribution without considering the Brownian diffusion effect gives the highest pressure drop.

For the case that both particle and pore sizes are of the Raleigh type distribution, and the Brownian diffusion

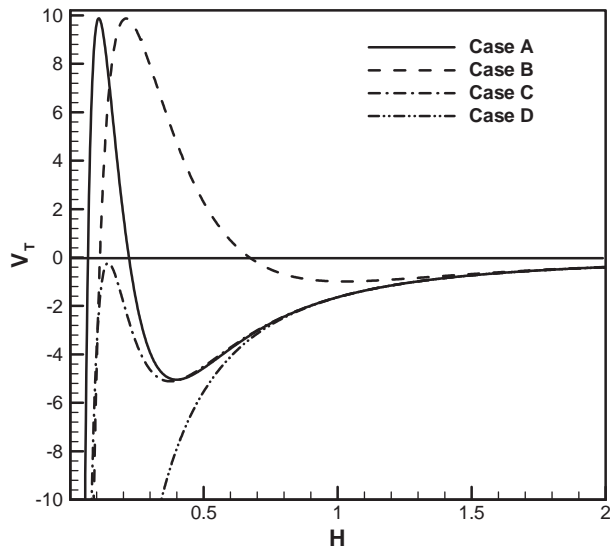


Fig. 5. Four types of total interaction energy curves adopted in the simulation of the present paper, at which $N_{E1} = 105.0$ and $N_{DL} = 10.75$ for curve A, $N_{E1} = 50.0$ and $N_{DL} = 5.02$ for curve B, $N_{E1} = 77.0$ and $N_{DL} = 10.0$ for curve C, $N_{E1} = 0.0$ and $N_{DL} = 0.0$ for curve D, and $N_{E2} = 1.0$ and $N_{L0} = 7.0$ for all four curves.

effect is included, Fig. 8 summarizes the simulation results of the permeability ratio K/K_0 versus pore volumes injected for these four different interaction energy curves shown in Fig. 5. As expected, the order of the magnitudes of K/K_0 in general is: curve D > curve C > curve B > curve A. Since there is no energy barrier exists, the mechanism of direct deposition becomes dominant in pores, hence the permeability ratio of curve D is always greater than that of the three other curves. Conversely, the permeability ratio of curve A is the lowest among the four curves because it has the steepest slope between the secondary minimum and the primary maximum, which causes more Brownian particles to block more of the small pores. The fact that the K/K_0 value of curve B is smaller than that of curve C implies that the height of the primary maximum plays a more important role in decreasing the deposition rate of particles than that of the depth of the secondary minimum.

5.2. Comparison with experimental data

Experimental data on temporal permeability reduction obtained by Soo and Radke (1984), Soo et al. (1986), and Stephan and Chase (2003) are adopted in the present paper to compare with the simulation results obtained from the above theoretical equations.

5.3. Data of Soo and Radke

For the experiments of Soo and Radke (1984) and Soo et al. (1986), they conducted a series runs of deep bed filtration with quartz sandpack columns (4.5 cm in length

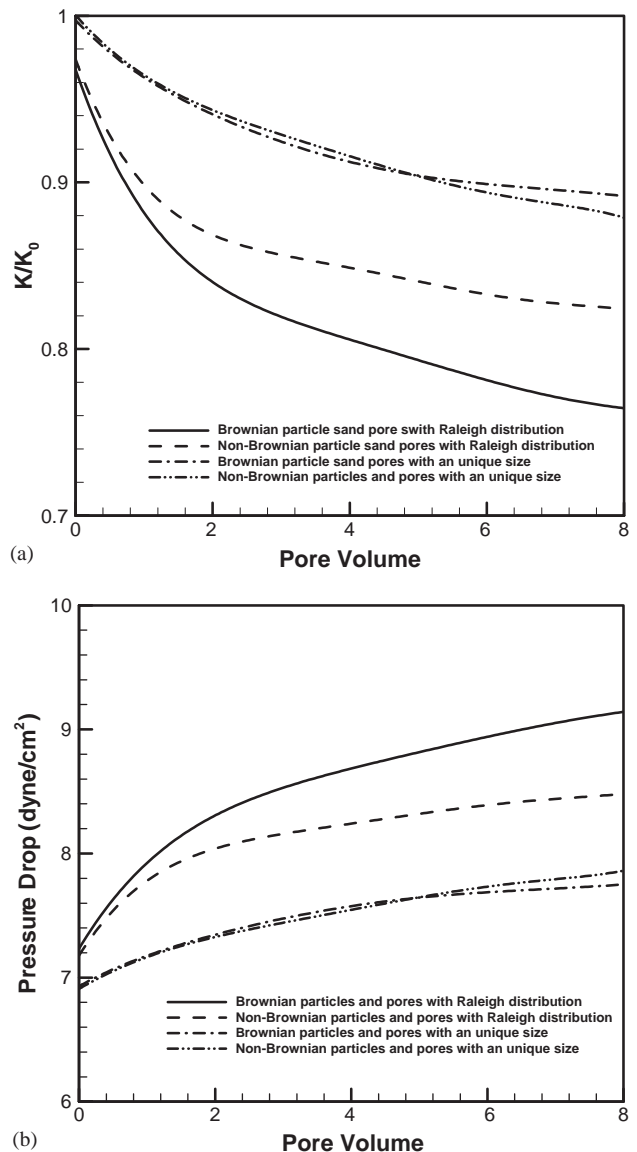


Fig. 6. (a) Effect of both particle and pore size distributions on the permeability ratio K/K_0 as the function of pore volumes injected, corresponding to curve A shown in Fig. 5. (b) The corresponded pressure drop obtained by using the present model.

and 2.1 cm in diameter), into which oil-in-water emulsions (Chevron 410H oil with a viscosity 15 mPa s) with different drop diameters were injected at a constant flow rate of $0.02 \text{ cm}^3/\text{s}$. In the present study, the drop sizes of 2.1 and $4.0 \mu\text{m}$ are adopted to compare with the above simulation method. The major experiment conditions used in the run of $2.1 \mu\text{m}$ oil drop size were (Soo and Radke, 1984): (a) the initial concentration of oil droplets in the emulsion C_{in} is 0.5 vol%, (b) the initial permeability of the sandpack column K_0 is $1.15 \mu\text{m}^2$, at which the porosity is 0.34 and (c) the mean pore diameter of the sandpack column is $29.5 \mu\text{m}$. Same experimental conditions were adopted for the run of $4.0 \mu\text{m}$ oil drop size, except that C_{in} is 0.6 vol% and K_0

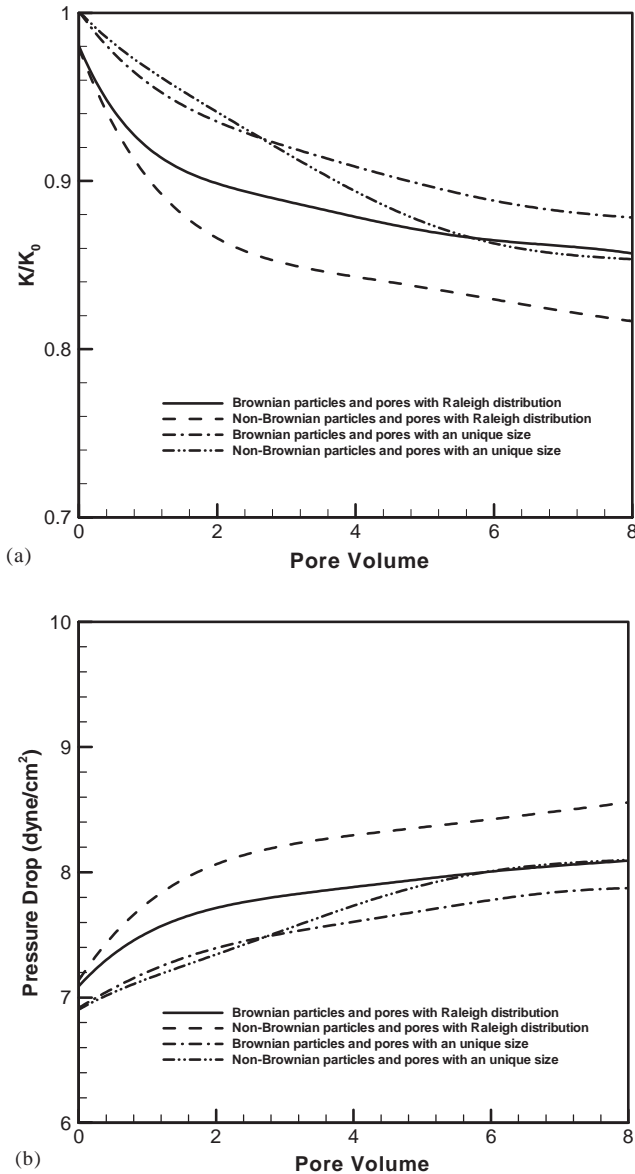


Fig. 7. (a) Effect of both particle and pore size distributions on the permeability ratio K/K_0 as the function of pore volumes injected, corresponding to curve D shown in Fig. 5. (b) The corresponded pressure drop obtained by using the present model.

is $2.0 \mu\text{m}^2$ (Soo et al., 1986). The zeta potentials of quartz sand grains and oil droplets in the pH 10.0 alkaline aqueous solution were reported to be -70.0 and -75.8 mV, respectively. The corresponded DLVO interaction energy curves for these two experiments are shown in Fig. 9a. Like curve B in Fig. 5, there is a significant primary maximum energy barrier exists between oil droplets and sand grains, which will cause more droplets to deposit at smaller pores in the filter as mentioned above. Applying these available experimental data, the simulation results of temporal permeability reduction are shown in Fig. 9b. Since lower permeability sandpack column owns higher oil droplets retention ability, hence the run of $2.1 \mu\text{m}$ drop size gives larger permeability

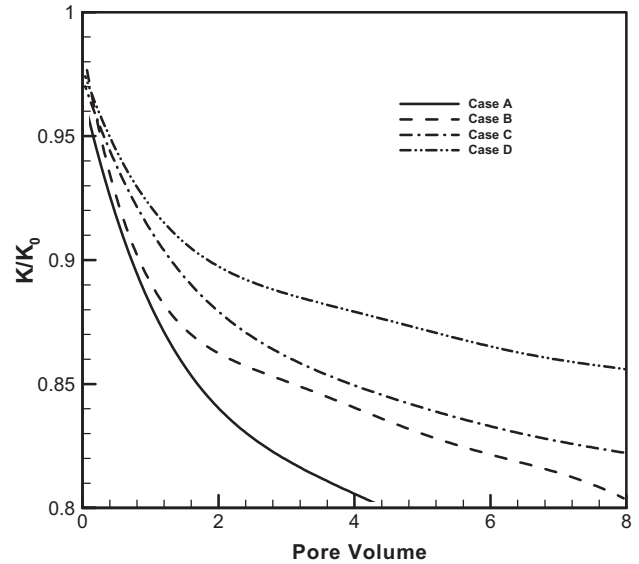
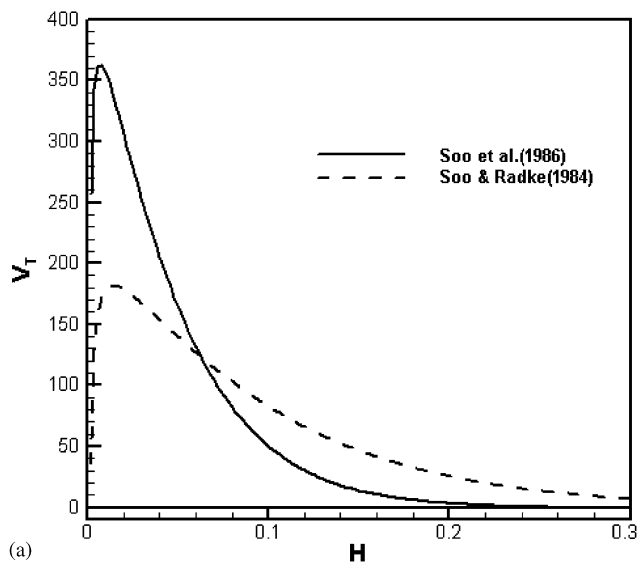


Fig. 8. Effect of the four different interaction energy curves shown in Fig. 5 on the permeability ratio K/K_0 as the function of pore volumes injected, when both the particle size and the pore size are all with Raleigh type distribution form on the permeability ratio K/K_0 as the function of pore volumes injected.

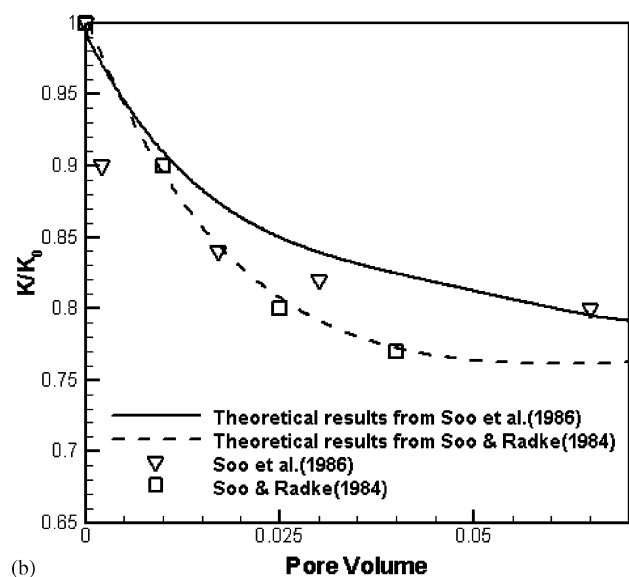
reduction at the steady state than that of the run of $4.0 \mu\text{m}$ drop size. More importantly, it is found that, because of the pronounced Brownian motion behavior, the run of $2.1 \mu\text{m}$ drop size gives a better agreement between the experiment data and the theoretical simulation than that of the run of $4.0 \mu\text{m}$ drop size.

5.4. Data of Stephan and Chase

In this study, Stephan and Chase (2003) had conducted a series runs of deep bed filtration experiments using Berea sandstone column (the average diameter of sand grains was $30.0 \mu\text{m}$), at which the combined effects of pH and salt concentration of injected Kaolinite clay suspension (average diameter of clay particles was $1.45 \mu\text{m}$) on the permeability reduction were investigated. The core was reported to have the dimension of 1.5 in diameter by 2.0 in length, and with a porosity of 0.163. The injection velocity of clay suspension was kept at $100 \text{ cm}^3/\text{h}$. Similar to the experiments of Khilar and Fogler (1984), the zeta potentials of clay particles and sand grains were found to have the values of -30.0 and -33.0 mV, respectively. When the salt concentration is kept at 0.07 M, the corresponded DLVO interaction energy curve is shown in Fig. 10a, at which a “barrierless” type curve is observed (like curve D in Fig. 5). Hence, the direct deposition of clay particles on pore walls will be the dominant mechanism in this experiment. A representative simulation result of temporal permeability reduction is shown in Fig. 10b, at which the concentration of injected suspension was kept at 15 mg/L. As shown in this figure, because the



(a)



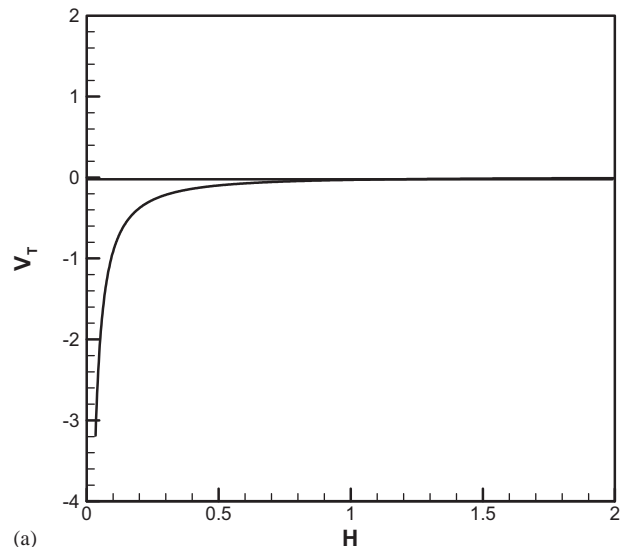
(b)

Fig. 9. (a) The corresponded interaction energy curves for the experimental data of Soo and Radke (1984) and Soo et al. (1986). (b) Comparison of the permeability ratio K/K_0 of theoretical results and the experimental data obtained by Soo and Radke (1984) and Soo et al. (1986) as the function of pore volumes injected.

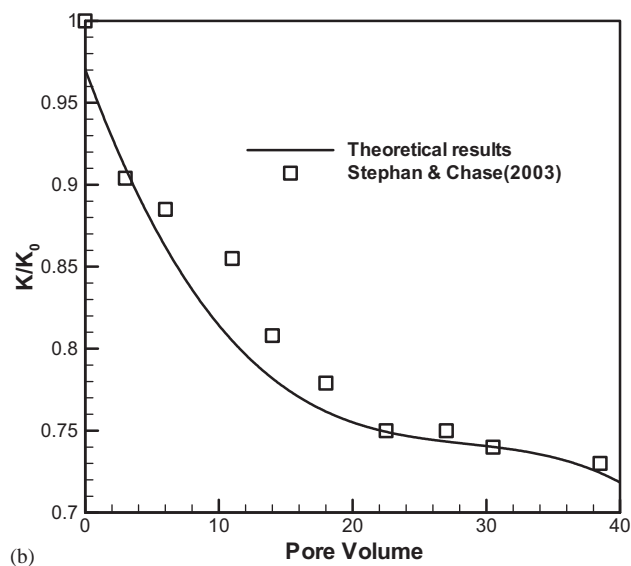
permeability reduction levels off to a steady value after 40 pore volumes of injection in this experiment, it is found that clay particles are captured throughout the filter bed mainly by the direct deposition mechanism and only a small amount of particles are captured by the straining mechanism.

6. Conclusion

The present simulation method can successfully predict the temporal permeability reduction by tracking the Brownian particles move through the filter bed. Our method also takes different size distributions of both particles and pores



(a)



(b)

Fig. 10. (a) The corresponded interaction energy curve for the experimental data of Stephan and Chase (2003). (b) Comparison of the permeability ratio K/K_0 of theoretical results and the experimental data obtained by Stephan and Chase (2003) as the function of pore volumes injected.

into account. The effects of the interaction energy curves of DLVO theory of various shapes were also investigated. Comparing with the available permeability reduction experimental data, it is found that our model can give a fair agreement between theory and experiments of Soo and Radke (1984, 1986) and Stephan and Chase (2003).

Since the present Brownian dynamics simulation method consumes a lot of computer time on tracking particles move through the filter bed, so we can only adopt the simple modified square network model in the present paper in order to save the computation time. But, this simplistic network model makes the present simulation method unable to predict the extreme drop in permeability (i.e. $K/K_0 \leq 0.5$) during the first few pore volumes of injection. Hence, in order

to resemble the real porous media, we will adopt more random nature network model (for example, the Voronoi type model) in our future simulation work. We will also adopt the three-stage block model established by Choo and Tien (1995) instead of using Eq. (19). This versatile model is believed being able to describe the degree of multi-layer adsorption of particles and cake formation on the pore walls more accurately, and therefore can make up the deficit of the present work.

Notation

a_i	the random number generated by using the standard computer software IMSL	N_L	the total number of bonds in the network defined as $A/6k_B T$
A	Hamaker constant	N_{LO}	
$A(t)$	Gaussian white noise process in stochastic terms	N_{Re}	Reynolds number, defined as $u_s d_f \rho_f / \mu$
C_{in}	influent particle concentration	$(N_{Re})_{avg}$	the averaged Reynolds number, defined by Eq. (26)
C_{eff}	effluent particle concentration	$(N_{Re})_i$	the local Reynolds number in the i th bond, defined by Eq. (25)
d_c	constriction diameter of a constricted tube	r_0	remotest radial position at the constriction tube inlet which can be reached by a particle
d_f	filter-grain diameter	r_c	constriction radius
d_{max}	maximum diameter of constricted tube	r_f	filter-grain radius
d_p	diameter of particle	r_{fi}	the local radius at the i th bond in the network
f_p	the dimensionless distribution density of pores	r_{f0}	the initial radius of the bond in the network
$F_1(H), F_2(H), F_3(H)$	retardation factors of normal vector, drag force, and shear vector, respectively	$r_{f_{new}}$	the local radius of the bond, defined by Eq. (19)
F_{DL}	dimensionless electrostatic repulsion force, defined by Eq. (9)	r_{in}	radial coordinate of the particle position at tube inlet
F_{LO}	dimensionless van der Waals force, defined by Eq. (8)	r_{max}	maximum radius of constriction tube
h	height of constricted tube	r_{mean}	the mean radius of pores
h_s	the smallest separation distance between the particle and the collector surface	r_p	particle radius
H	defined as h_s/r_p	r_{pm}	the mean radius of particles
k_B	Boltzman constant	r_w	wall radius
K	the overall permeability of the filter, defined by Eq. (22)	r'	the dimensionless radius of pores
K_i	the local permeability in the i th bond, defined by Eq. (20)	r'_1	the dimensionless radius, defined as r_f/r_{mean}
K_0	the initial permeability of the filter	$R_v(t)$	random deviates of velocity increment due to Brownian motion, which are bivariate-Gaussian distribution
K_1	constant, defined by Eq. (16)	$R_r(t)$	random deviates of displacement increment due to Brownian motion, which are bivariate Gaussian distribution
l_f	length of the unit bed element	S_{wi}	fraction of saturation
L	length of the filter bed	t	time
m_p	mass of the particle	T	absolute temperature
N_c	number of unit cells per unit cross-sectional area	u_s	superficial velocity
N_{DL}	double-layer force parameter, defined as κr_p	u_i	the local velocity of fluid at the i th bond in the network
N_{E1}	first electrokinetic parameter, defined as $vr_p(\varphi_1^2 + \varphi_2^2)/4k_B T$	U	uniform velocity entering constriction tube
N_{E2}	second electrokinetic parameter, defined as $2 \left(\frac{\varphi_1}{\varphi_2} \right) / \left[1 + \left(\frac{\varphi_1}{\varphi_2} \right)^2 \right]$	U_{in}	the influent flow rate
		V	particle velocity vector
		V_f	total void space in the filter
		V_p	total volume of deposited particles in the filter
		V_0	initial velocity of V
		Z	particle position vector
		Z_0	initial value of Z
		<i>Greek letters</i>	
		β	friction coefficient per unit mass of particle
		ΔP_{total}	the total pressure drop through the bond, defined by Eq. (17)

ΔP_p	the pressure drop caused by the deposited particle in the bond, defined by Eq. (15)
ΔP_{tube}	the pressure drop of fluid through the bond, defined by Eq. (18)
ε	filter porosity
ε_i	the local porosity at the i th bond, defined by Eq. (21)
ϕ_{DL}	dimensionless van der Waals attractive energy
ϕ_{Lo}	dimensionless electrostatic repulsive energy
φ_1, φ_2	surface (zeta) potentials of particle and collector, respectively
θ_{in}	angular coordinate of the particle position at tube inlet
κ	reciprocal of the electric double layer thickness
μ	viscosity of fluid
ν	dielectric constant of the fluid
ρ_f	density of fluid
<i>Other symbol</i>	
$\langle \rangle$	average value

Acknowledgements

The authors would like to express their sincere thanks to Profs. Chi Tien at Chemical Engineering Department of Syracuse University for his valuable suggestions on this work. The financial support received from the National Science Council of the Republic of China, research grant no. NSC-91-2214-E-029-00, is greatly appreciated.

References

- Burganos, V.N., Paraskeva, C.A., Payatakes, A.C., 1992. Three-dimensional trajectory analysis and network simulation of deep bed filtration. *Journal of Colloid and Interface Science* 148 (1), 167–181.
- Chang, Y.I., Whang, J.J., 1998. Deposition of Brownian particles in the presence of energy barriers of DLVO theory: effect of the dimensionless groups. *Chemical Engineering Science* 53 (23), 3923–3939.
- Chang, Y.I., Chen, S.C., Lee, E., 2003. Prediction of Brownian particle deposition in porous media using the constricted tube model. *Journal of Colloid and Interface Science* 266 (1), 48–59.
- Chiang, H.W., Tien, C., 1985. Dynamics of deep-bed filtration: Part I. Analysis of two limiting situations. *A.I.Ch.E. Journal* 31 (8), 1349–1359.
- Choo, C.U., Tien, C., 1995. Simulation of hydrosol deposition in granular media. *A.I.Ch.E. Journal* 41 (6), 1426–1442.
- Chow, J.C.F., Soda, K., 1972. Laminar flow in tubes with constriction. *The Physics of Fluids* 15 (10), 1701–1706.
- Elimelech, M., 1994. Particle deposition on ideal collectors from dilute flowing suspensions: mathematical formulation, numerical solution, and simulations. *Separation Technology* 4, 186–212.
- Fedkiw, P., Newman, J., 1977. Mass transfer at high Peclet number for creeping flow in a packed-bed reactor. *A.I.Ch.E. Journal* 23 (3), 255–263.
- Gupta, D., Peters, M.H., 1985. A Brownian dynamics simulation of aerosol deposition onto spherical collectors. *Journal of Colloid and Interface Science* 104 (2), 375–389.
- Happel, J., Brenner, H., 1983. *Low Reynolds Number Hydrodynamics*. Martinus Nijhoff, Boston. (Chapter 7).
- Herzig, J.P., Leclerc, D.M., LeGoff, P., 1970. Flow of suspension through porous media—application in deep bed filtration. *Industrial and Engineering Chemistry* 62 (1), 8–35.
- Imdakh, A.O., Sahimi, M., 1991. Computer simulation of particle transport processes in flow through porous media. *Chemical Engineering Science* 46 (8), 1977–1993.
- IMSL Libraries, 1985. IMSL, Houston, TX.
- Ison, C.R., Ives, K.J., 1969. Removal mechanisms in deep bed filtration. *Chemical Engineering Science* 24 (2), 717–729.
- Kanaoka, C., Emi, H., Tarthapanichakoon, W., 1983. Convective diffusional deposition and collection efficiency of aerosol on a dust-loaded fiber. *A.I.Ch.E. Journal* 29 (6), 895–902.
- Khilar, K.C., Fogler, H.S., 1984. The existence of a critical salt concentration for particle release. *Journal of Colloid and Interface Science* 101 (1), 214–224.
- Kim, J.S., Rajagopalan, R., 1982. A comprehensive equation for the rate of deposition of colloidal particles and for stability ratios. *Colloids Surfaces* 4 (1), 17–31.
- Kirkpatrick, S., 1973. Percolation and conduction. *Review in Modern Physics* 45 (4), 574–588.
- Payatakes, A.C., Tien, C., Turian, R.M., 1973. A new model for granular porous media: Part I. Model formulation. *A.I.Ch.E. Journal* 19 (1), 58–67.
- Pendse, H., Tien, C., Rajagopalan, R., Turian, R.M., 1978. Dispersion measurement in clogged filter beds: a diagnostic study on the morphology of particle deposits. *A.I.Ch.E. Journal* 24 (3), 473–485.
- Prieve, D.C., Ruckenstein, E., 1974. Effect of London forces upon the rate of deposition of Brownian particles. *A.I.Ch.E. Journal* 20 (6), 1178–1187.
- Ramarao, B.V., Tien, C., Mohan, S., 1994. Calculation of single fiber efficiencies for interception and impaction with superposed Brownian motion. *Journal of Aerosol Science* 25 (2), 295–313.
- Rajagopalan, R., 1974. Stochastic modeling and experimental analysis of particle transport in water filtration. Ph.D. Dissertation, Syracuse University, Syracuse, New York (Chapters 4–6).
- Rege, S.D., 1988. A network model for flow, reaction, and particle entrapment in porous media. Ph.D. Dissertation, University of Michigan, Ann Arbor, MI (Chapter 3).
- Rege, S.D., Fogler, H.S., 1988. A network model for deep bed filtration of solid particles and emulsion drops. *A.I.Ch.E. Journal* 34 (11), 1761–1772.
- Russel, W.B., Saville, D.A., Schowalter, W.R., 1989. *Colloids Dispersions*. Cambridge University Press, Cambridge. (Chapter 3).
- Sahimi, M., Gavalas, G.R., Tsotsis, T.T., 1990. Statistical and continuum models of fluid-solid reactions in porous media. *Chemical Engineering Science* 45 (6), 1443–1502.
- Sharma, M.M., Yortsos, Y.C., 1987. A network model for deep bed filtration processes. *A.I.Ch.E. Journal* 33 (10), 1644–1653.
- Soo, H., Radke, C.J., 1984. The flow mechanism of dilute, stable emulsions in porous media. *Industrial and Engineering Chemistry Fundamentals* 23 (3), 342–347.
- Soo, H., Williams, M.C., Radke, C.J., 1986. A filtration model for the flow of dilute stable emulsions in porous media—II. Parameter evaluation and estimation. *Chemical Engineering Science* 41 (2), 273–281.
- Spielman, L.A., FitzPatrick, J.A., 1973. Theory for particle collection under London and gravity forces. *Journal of Colloid and Interface Science* 42 (3), 607–623.
- Spielman, L.A., Friedlander, S.K., 1974. Role of electric double layer in particle deposition by convective diffusion. *Journal of Colloid and Interface Science* 46 (1), 22–31.
- Stephan, E.A., Chase, G.G., 2003. Use of genetic algorithms as an aid in modeling deep bed filtration. *Computer & Chemical Engineering* 27 (1), 281–292.
- Tien, C., 1989. *Granular Filtration of Aerosols and Hydrosols*. Butterworths, Boston (Chapters 3–5).

- Tien, C., Payatakes, A.C., 1979. Advances in deep bed filtration. *A.I.Ch.E. Journal* 25 (5), 737–759.
- Todd, A.C., Somerville, J.E., Scott, G., 1984. The application of depth of formation damage measurements in predicting water injectivity decline. SPE, No. 12498, Denver, CO.
- Verwey, E.J.W., Overbeek, J.Th.G., 1948. *Theory of the Stability of Lyophobic Colloids*. Elsevier, Amsterdam.
- Wang, C.S., Beizaie, M., Tien, C., 1977. Deposition of solid particles on a collector: formulation of a new theory. *A.I.Ch.E. Journal* 23 (6), 879–889.
- Yao, K.M., Habidian, M.T., O'Melia, C.R., 1977. Water and waste water filtration: concepts and applications. *Environmental Science and Technology* 5 (11), 1105–1116.